Published in final edited form as:

Cell Rep. 2026 May 26; 45(5): 117291. doi:10.1016/j.celrep.2026.117291.

SFPQ prevents MDA5-mediated activation of innate immunity and preserves cell viability

Huirong Zhang[1,2], **Runjie Yuan**[1,2], **Praneet K. Sandhu**[1,2], **Justin T. Landis**[1], **Dirk P. Dittmer**[1,2], **Blossom Damania**[1,2,3,*]

[1]Lineberger Comprehensive Cancer Center, University of North Carolina at Chapel Hill, Chapel Hill, NC, USA

[2]Department of Microbiology and Immunology, University of North Carolina at Chapel Hill, Chapel Hill, NC, USA

[3]Lead contact

SUMMARY

The melanoma differentiation-associated gene 5 (MDA5) sensor recognizes double-stranded RNA (dsRNA) produced during viral infections, leading to type I interferon (IFN) production. Host proteins can shield endogenous dsRNA from MDA5 through RNA modifications, such as A-to-I editing of dsRNA by adenosine deaminase acting on RNA 1 (ADAR1). The splicing factor proline- and glutamine-rich (SFPQ) is an RNA-binding protein that regulates RNA biogenesis. However, its role in innate immunity has not been previously explored. We report that SFPQ can promote viral replication of Kaposi's sarcoma-associated herpesvirus (KSHV) and demonstrate that SFPQ can prevent IFN production not only in the context of viral replication but also in uninfected cells. Furthermore, SFPQ associates with ADAR1 and modulates A-to-I editing of cellular RNA transcripts. Moreover, SFPQ depletion in uninfected cells induced IFN response genes, including MDA5 and ZBP1, and impaired cell growth. In summary, SFPQ binds ADAR1

*Correspondence: damania@med.unc.edu.

AUTHOR CONTRIBUTIONS

H.Z. designed the experiments, performed the experiments, and prepared the manuscript. R.Y. performed the viral infections and plaque assays. P.K.S. assisted with the IFA experiment. J.T.L. and D.P.D. analyzed the RNA-seq data. B.D. designed the study, obtained funding, and helped write and edit the manuscript.

DECLARATION OF INTERESTS

The authors declare no competing interests.

RESOURCE AVAILABILITY

Lead contact

Further information and requests for resources and reagents should be directed to and will be fulfilled by the lead contact, Blossom Damania (damania@med.unc.edu).

Materials availability

A materials transfer agreement will be needed for procuring reagents in this manuscript.

Data and code availability

- RNA-seq and whole genome sequencing data were deposited in the NCBI BioProject database :https://www.ncbi.nlm.nih.gov/bioproject, accession number PRJNA1433810.
- This paper does not report original code.
- Any additional information required to reanalyze the data reported in this paper is available from the lead contact upon request.

and modulates its editing function, thereby preventing cellular RNAs from activating MDA5-mediated innate immune responses.

Graphical Abstract

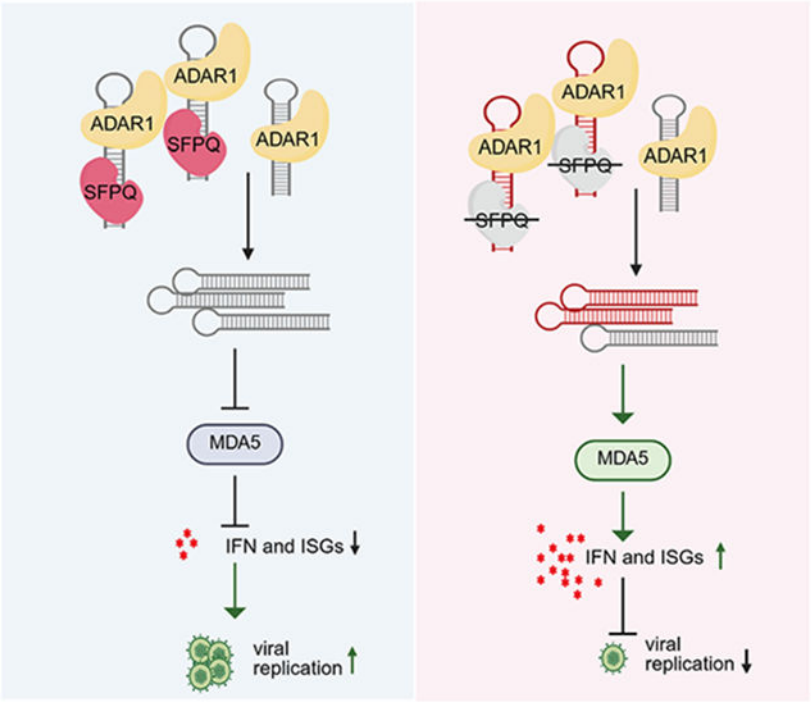

In brief

In this study, Zhang et al. demonstrate that SFPQ is a proviral factor that facilitates KSHV lytic reactivation. By interacting with ADAR1, SFPQ modulates its A-to-I editing efficiency to suppress MDA5-mediated innate immune responses. SFPQ depletion induced IFN response genes, including MDA5 and ZBP1, and impaired cell growth.

INTRODUCTION

Host cells initiate innate immune responses upon recognition of pathogen-associated molecular patterns (PAMPs) by diverse pattern recognition receptors (PRRs). These PRRs are located in different subcellular compartments and include endosomal Toll-like receptors (TLRs), cytosolic DNA sensor cyclic GMP-AMP synthase (cGAS), and RNA-sensing retinoic acid-inducible gene I protein (RIG-I)-like receptors (RLRs).[1]The RLRs encompass two major RNA receptors: RNA helicases, like retinoic acid-inducible gene I (RIG-I; also known as DDX58) and melanoma differentiation-associated gene 5 (MDA5; also known as IFIH1). Upon binding to RNA ligands, RIG-I/MDA5 are activated and interact with their adaptor protein, the mitochondrial antiviral signaling (MAVS) protein, to induce the RLR signaling pathway and subsequently produce type I interferon (IFN) and proinflammatory cytokines.[2] Type I IFN signaling then activates the Janus kinase-signal transducer and

activator of transcription (JAK/STAT) pathway, leading to transcription of hundreds of ISGs to establish an antiviral state.[3]

SFPQ, also known as PTB-associated splicing factor (PSF), is an RNA-binding protein (RBP) that plays multiple roles with respect to RNA biogenesis, including in transcription, splicing, and intracellular trafficking.[4,5] It interacts with RNA polymerase II, functioning in the initiation and elongation stages of transcription.[6] SFPQ also regulates circular RNA biogenesis and cryptic last exon (CLE) formation by affecting RNA splicing.[7,8] It is a critical component of cytoplasmic RNA transport granules and is involved in nuclear retention of RNAs within subnuclear sequestration of SFPQ complexes.[9,10] SFPQ functions as a repressor of transcription of IL-8 and the NF-κB subunit, RelA, through its binding activity with long non-coding RNAs (lncRNAs).[11,12] In addition to its role in regulating cellular RNA, SFPQ modulates the transcription and replication of some RNA viruses, including influenza A[13] and rhinovirus.[14] However, its role in innate immune responses to viral infection has not been explored.

Kaposi's sarcoma-associated herpesvirus (KSHV) is an oncogenic double-stranded DNA (dsDNA) virus exhibiting two distinct phases in its life cycle: latency and lytic replication. During latency, KSHV expresses only a limited number of latency-associated genes. During lytic reactivation, all viral genes are transcribed to produce progeny virions.[15,16] KSHV lytic infection produces virus- and host-derived RNAs with double-stranded structures, such as miRNAs and long noncoding RNAs.[17-20] Consequently, several RNA-binding proteins (RBPs) have been identified that facilitate viral DNA replication through inhibition of the innate immune sensors, RIG-I and MDA5. We previously reported that an RNA editing enzyme, adenosine deaminase acting on RNA 1 (ADAR1), aids KSHV replication through inhibition of the IFN I response.[17,21] In this study, we screened RBPs for their ability to regulate KSHV replication and the innate immune response during viral lytic reactivation. We identified that SFPQ inhibits type I IFN responses and facilitates KSHV lytic replication. We report that SFPQ associates with ADAR1 in an RNA-dependent manner, as a reduction in their association was observed in co-immunoprecipitation experiments treated with RNase. Moreover, we found that the A-to-I editing frequency was decreased in SFPQ-depleted cells. We also found that SFPQ prevented cellular RNAs from triggering an innate immune response. Loss of SFPQ activated the double-stranded RNA (dsRNA) sensor, MDA5, and type I IFN response genes, while combined depletion of SFPQ with MDA5 or its adapter MAVS reversed this activation. In summary, SFPQ prevents MDA5-mediated innate immune responses in an ADAR1-dependent manner.

RESULTS

SFPQ facilitates viral replication during KSHV lytic reactivation

To identify RBPs that affect KSHV replication, we performed a siRNA screen in iSLK.219 cells by targeting 64 RBPs during KSHV lytic reactivation. iSLK.219 cells contain a latent KSHV genome and a doxycycline (Dox)-inducible RTA (replication and transcription activator) protein.[22] Induction of RTA initiates viral lytic reactivation and lytic replication.[22,23] The viral episome in iSLK.219 cells also express a constitutive GFP marker and an RFP marker under the control of a lytic cycle-specific promoter, which

was used as an indicator for reactivating cells.[22] The RFP intensity serves as a readout for lytic reactivation, with changes in RFP intensity upon RBP knockdown indicating that the targeted RBP is likely crucial for viral replication during KSHV lytic reactivation. Compared to control cells treated with a non-specific siRNA, depletion of several RBPs affected RFP intensity after Dox treatment. A knockdown of activating signal cointegrator 1 complex subunit 1 (ASCC1), heterogeneous nuclear ribonucleoprotein A1 (HNRNPA1), ADAR1, DEAD-box helicase 3 X-linked (DDX3X), or SFPQ decreased RFP intensity, while the RFP intensity was increased in Exportin-1 (XPO-1)-, up-frame-shift-1 (UPF1)-, transforming growth factor beta regulator 4 (TBRG4)-, or interleukin enhancer binding factor 3 (ILF3)-depleted cells (ratio >10:1 in Figures 1A and 1B). We also measured IFNβ in the supernatant when performing the RBP screening assay. Based on our prior work, ADAR1 served as a positive control.[21] In addition to ADAR1-depletion, knockdown of SFPQ was the only other candidate RBP that also induced IFNβ after Dox treatment (Figure 1C). Taken together, these data indicate that SFPQ may play an important role in regulating innate immune responses and viral replication during RTA-induced KSHV lytic reactivation.

To confirm the role of SFPQ in KSHV lytic reactivation, we knocked out SFPQ in iSLK.219 cell lines using CRISPR-Cas gene-editing technology and induced KSHV lytic replication with Dox-induced RTA. The knockout efficiency of SFPQ was confirmed by western blot (Figure 1D). While the expression of the lytic KSHV genes vIL-6, ORF45, and K8a was successfully induced upon reactivation, SFPQ-depleted cells showed an impaired ability to induce KSHV lytic proteins compared to control cells. This was also confirmed by observing RFP expression (Figures 1E and 1F) and measuring KSHV lytic mRNA transcripts by real-time quantitative polymerase chain reaction (RT-qPCR) (Figures 1H-1J). We performed RNA-sequencing (RNA-seq) profiles on control and SFPQ-depleted iSLK.219 with and without Dox-induced lytic reactivation to investigate the regulation of SFPQ during viral replication. An independent analysis of viral transcription by RNAseq showed the same pattern (Figure 1G). Dox treatment induced KSHV gene expression genome-wide in NTC (non-targeting control) transfected control cells, but SFPQ depletion significantly decreased the transcriptional level of viral genes during KSHV lytic reactivation (Figure 1G; Data S1).

To confirm the role of SFPQ in a second, independent cell line, the experiments were repeated in TREx BCBL1-RTA cells, a KSHV-infected PEL-derived B cell line.[24] Like iSLK.219 cells, TREx BCBL1-RTA cells carry an RTA gene under the control of a Dox-inducible promoter. Here too, depletion of SFPQ by shRNA significantly decreased the mRNA transcription and protein expression level of multiple KSHV lytic genes (Figures S1A-S1D). These data demonstrate that SFPQ serves as a proviral factor during KSHV lytic reactivation.

To evaluate whether SFPQ knockdown affects Dox-induced RTA expression, we transfected NTC or SFPQ siRNA in iSLK.RTA cells, which harbor a Dox-inducible RTA gene but lack the KSHV genome, and then treated with Dox (Figure S2A). As expected, Dox treatment increased both RTA protein and mRNA levels, but SFPQ knockdown did not alter RTA expression at either protein or mRNA level compared with NTC control cells (Figures S2B and S2C). Therefore, SFPQ depletion has no effect on Dox-induced RTA expression.

SFPQ prevents type I IFN signaling and ISG induction during KSHV lytic reactivation

Since depletion of SFPQ induced a significant IFN response (Figure 1), we wanted to broadly confirm the role of SFPQ in innate immunity during KSHV lytic reactivation. The expression of IFNβ mRNA and protein was increased in SFPQ KO cells compared to NTC cells upon Dox treatment (Figures 2A and 2B). In general, IFNβ can be induced through phosphorylation and activation of TBK1 and IRF3.[25] We found that the knockout of SFPQ significantly increased phosphorylation of IRF3 and TBK1 (Figure 2C) in both KSHV latent infection (dimethyl sulfoxide [DMSO]-treated cells) and lytic reactivation induced by Dox treatment (Figure 2C). Unlike IFN levels, pTBK1 levels were not further increased in reactivated cells compared with latently infected cells following SFPQ KO. Since IκB kinase ε (IKKε) has been shown to phosphorylate IRFs and other downstream effectors,[1,26] it is possible that during KSHV reactivation and in the absence of SFPQ, IKKε activation also leads to IRF3 phosphorylation and ISG induction in a TBK1-independent manner.

RNA-seq analysis showed upregulation of many transcripts in SFPQ-depleted cells compared to control cells. Among the most significantly changed mRNAs, several were functionally linked to type I IFN responses, such as IFIH1, IFIT1, IFIT3, ISG15, and OAS2 (Figure 2D). Gene Ontology (GO) analysis showed that the expression of genes in the SFPQ-depleted cells was enriched in the type I IFN signaling pathway versus the control cells (Figure 2E). Comparison of IFN-stimulated genes (ISGs) from the RNA-seq data identified a set of 82 genes that were induced when SFPQ was depleted at baseline. KSHV lytic reactivation further elevated these in SFPQ-depleted cells compared to control cells (Figure 2F; Data S2). RT-qPCR analysis independently confirmed the upregulation of selected ISGs, including OAS2, MX2, ISG15, and IFIT3 in SFPQ knockout cells compared with control cells (Figures 2G-2J). Taken together, the data indicate that the loss of SFPQ significantly activates the IFN signaling pathway and induces ISG expression.

To investigate whether SFPQ facilitates KSHV lytic reactivation by inhibiting innate immune responses, we transfected iSLK.219 cells with SFPQ siRNA alone or together with IRF3 siRNA and then induced lytic reactivation with Dox and measured RFP induction. As before, the depletion of SFPQ significantly reduced RFP-positive cells, an indicator of KSHV lytic reactivation, compared with control cells (Figures 2L and S3A). This phenotype was slightly rescued by a knockdown of IRF3 in SFPQ-depleted cells. The number of RFP-positive cells increased compared with the knockdown of SFPQ alone (Figures 2L and S3A). Likewise, the induction of ISGs in SFPQ-deficient cells was abolished by concurrent depletion of IRF3 and SFPQ (Figures 2M and S3B). Concomitantly, KSHV gene expression was reduced in SFPQ-depleted cells but partially rescued by depletion of SFPQ and IRF3 together (Figures 2K and S3C-S3E).

SFPQ associates with ADAR1p110 and ADAR1p150 isoforms and affects A-to-I RNA editing

It has been reported that SFPQ is able to bind inosine-containing RNAs, which are mainly edited by ADAR1 in mammalian cells.[9] This suggests a relationship between SFPQ and ADAR1 function. To test this hypothesis, we first confirmed the subcellular localization of SFPQ and ADAR1 in KSHV reactivated cells. Both endogenous SFPQ and ADAR1

proteins were found to be expressed and localized in the nucleus (Figure 3A). To validate the direct interaction between SFPQ and ADAR1, we performed co-immunoprecipitation using anti-SFPQ or negative-control IgG to see if ADAR1 interacted with SFPQ. ADAR1 has two isoforms, ADAR1p110 and ADAR1p150 (Figure 3B). Both ADAR1 isoforms were pulled down using an antibody against SFPQ. Conversely, SFPQ was pulled down using an antibody against ADAR1 but not the control IgG antibody (Figure 3C). ADAR1p150 is normally expressed in low quantities, but it is induced by IFN. The SFPQ-ADAR1 association was increased in the presence of IFNβ (Figure 3C).[27] Paraspeckle protein component 1 (PSPC1, also known as PSP1), a known interactor of SFPQ, served as a positive control (Figure 3C). To further verify the association between SFPQ and ADAR1, we treated the cells with IFNβ to increase the levels of ADAR1 protein expression and then performed the same IP as described earlier. More ADAR1p150 was detected with SFPQ in IFNβ-treated cells than in untreated mock cells (Figure 3C). Similarly, an immuno-precipitation assay was performed with anti-ADAR1 or negative-control IgG, and immunoblotting showed that SFPQ was also pulled down by ADAR1 but not by the negative control IgG (Figure 3C).

We next investigated whether the association between SFPQ and ADAR1 was dependent on RNA. Following treatment with IFNβ, we performed an immunoprecipitation assay with anti-SFPQ and treated half of each immunoprecipitated complex with RNase A. PSPC1 is known to interact with SFPQ in an RNA-independent manner and was used as a control. Immunoblotting showed that RNase A treatment had no effect on the interaction between SFPQ and PSPC, but the association between SFPQ and ADAR1 was completely abolished in RNase-treated immunoprecipitates (Figure 3D). Taken together, these results indicate that the association between SFPQ and both ADAR1 isoforms occurs in an RNA-dependent manner.

SFPQ is a multidomain protein that includes both DNA and RNA binding sites.[28] To identify the domain of SFPQ protein responsible for its association with ADAR1, we performed IP analysis by transfecting and overexpressing HA-tagged SFPQ truncated mutants to pull down endogenous ADAR1 in HEK293T cells (Figure 3B). Consistent with the aforementioned results of endogenous SFPQ immunoprecipitation, HA-tagged full-length SFPQ pulled down both endogenous ADAR1 isoforms (Figure 3E). The HA-tagged SFPQ mutant lacking the first RNA-binding domain, RRM1, still pulled down ADAR1, while SFPQ lacking RRM2 lost the association with ADAR1 (Figure 3E). Moreover, the SFPQ mutant lacking both RRM1 and RRM2 also failed to pull down either endogenous ADAR1 or exogenous ADAR1 (Figures 3E and 3F). In addition to loss of the RRM2 domain, the absence of the N-terminal DNA binding domain of SFPQ also resulted in the loss of association with ADAR1 (Figure 3E). These findings indicate that both the RRM2 and DBD domains of SFPQ are necessary for its association with ADAR1.

Our whole genome and RNA-seq analysis of iSLK.219 cells identified 33 statistically significant ($p < 0.05$) A-to-I editing sites with altered G levels in SFPQ siRNA (siSFPQ)-depleted cells compared to NTC siRNA (siNTC) controls (Data S4). We further report a total of 62 sites showing differences in editing levels between the siNTC and siSFPQ samples with $p < 0.1$. To validate the effects of SFPQ on A-to-I editing efficiency, we chose

five transcripts that undergo A-to-I editing based on our RNA-seq data and previous reports (Figure 3G; Data S4). In this study, we identified A-to-I editing transcripts in NEAT1, ARHGAP26, SNRPD3, SDHAF4, and ZNF488 (Table S1). Vlachogiannnis et al. previously reported that NEAT1 undergoes A-to-I editing.[29] The editing sites in the transcripts of ARHGAP26[30] and SNRPD3[31] have been previously predicted by RNA-seq analysis, whereas the A-to-I editing in SDHAF4 and ZNF488 is reported in this study. We confirmed the editing events of NEAT1, ARHGAP26, SNRPD3, SDHAF4, and ZNF488 by comparing the genomic and transcript sequences using PCR amplification of cDNA followed by Sanger sequencing. We noted that the inosine-edited transcripts were significantly detected in the cDNA of all five genes, while the relative amount of edited transcript for these genes decreased dramatically in SFPQ-depleted cells compared to NTC control cells (Figure 3G). As a positive control, a knockout of ADAR1 resulted in a complete loss of inosine-edited transcripts for all five genes in human umbilical vein endothelial cells (HUVECs) (Figure 3G). Taken together, our data suggest that SFPQ associates with ADAR1 and can affect the A-to-I editing efficiency of RNA transcripts mediated by ADAR1 (Figure S4).

Loss of SFPQ induces basal type I IFN response in uninfected cells

Since the knockout of SFPQ could induce ISGs in KSHV-infected cells, we wanted to investigate whether SFPQ has an impact on basal cellular type I IFN in the absence of virus. We used uninfected HUVEC cells and first checked the induction of ISGs after SFPQ knockout. As shown in Figures 4A-4F, the knockout of SFPQ significantly induced the mRNA expression of IFNβ, IFIH1, interferon-induced protein with tetratricopeptide repeat 1 (IFIT1), interferon-induced protein with tetratricopeptide repeat 3 (IFIT3), Z-DNA-binding protein (ZBP1), and C-X-C motif chemokine ligand 10 (CXCL10/IP-10) compared to NTC (Figures 4A-4F). There was more CXCL10 protein produced in the supernatant in SFPQ KO cells than in control cells (Figure 4G). In addition, protein levels of the dsRNA sensor MDA5 (IFIH1) were markedly increased in SFPQ knockout cells (Figure 4H), and the MDA5-regulated proteins IRF3, TBK1, and STAT1 were activated when cells were transfected with sgRNAs targeting SFPQ (Figure 4H). Protein expression levels of IFIT1 and IFIT3 were also increased in SFPQ-depleted cells (Figure 4H). We then profiled 84 type I IFN response genes by RT-qPCR array (Qiagen, GeneGlobe ID: PAHS-016Z). Forty-seven showed higher induction (>2-fold) in SFPQ-depleted cells than in control cells. The overall gene expression profile of the 84 genes tested is shown as a heatmap in Figure 4I, and the raw data are provided in Data S3. In addition to MDA5, another innate immune sensor, ZBP1 (also known as DAI and DLM-1), had increased mRNA levels in SFPQ-depleted cells (Figures 4E and S4). ZBP1 protein expression was readily detected in SFPQ-depleted cells upon IFNβ treatment, but not in NTC-transfected cells (Figures S4A and S4B). Moreover, the innate immune response was further enhanced in SFPQ-depleted endothelial cells during infection with Vesicular Stomatitis virus (VSV) (Figures S5A-S5F). Consistent with this response, VSV replication in endothelial cells was reduced in SFPQ-depleted cells compared to NTC control cells (Figure S5G).

Both dsRNA and Z-RNA are known ligands that activate MDA5 and ZBP1, respectively. To determine whether SFPQ depletion induces the formation of dsRNA or Z-RNA, we knocked down SFPQ in HUVEC and visualized dsRNA and Z-RNA using the J2 antibody

and Z-RNA antibody, respectively. Our results showed that while SFPQ depletion led to an accumulation of dsRNA, Z-RNA was not detected (Figures S6A-S6C).

To establish the robustness of this phenotype, we conducted several control experiments. We first evaluated ADAR1 depletion in HUVEC and found that innate immune signaling was strongly induced in HUVEC when ADAR1 was depleted (Figures S7A-S7G). In contrast, ADAR2 knockdown did not affect the innate immune response (Figures S7A-S7G). To determine whether knockdown of SFPQ in ADAR1-depleted cells could further enhance the IFNβ induction, we knocked down SFPQ in ADAR1-deficient cells. IFNβ production did not increase beyond the level observed with ADAR1 knockdown alone. These results suggest that SFPQ and ADAR1 may act on overlapping RNA substrates that contribute to MDA5 activation and IFNβ induction (Figure S8).

Both SFPQ and ADAR1 facilitate KSHV lytic replication, and both are negative regulators of ZBP1 activation. To determine whether ZBP1 influences KSHV replication, we first noted that the basal level of ZBP1 is very low in iSLK.219 cells. Therefore, we used IFNβ to induce ZBP1 expression in NTC control and ZBP1 siRNA–transfected cells, followed by induction of KSHV lytic reactivation. Upon IFNβ treatment, ZBP1 expression was robustly induced in NTC cells but remained low in ZBP1 siRNA–transfected cells (Figure S9A). IFNβ treatment reduced viral replication, while knockdown of ZBP1 did not alter viral levels compared with NTC control cells (Figures S9B-S9F). Together, these results indicate that IFN-induced ZBP1 does not affect KSHV lytic reactivation.

SFPQ belongs to a conserved family of multifunctional nuclear factors termed DBHS (Drosophila behavior human splicing) proteins, which also includes human non-POU domain-containing octamer-binding protein (NONO, also known as p54nrb) and PSPC1. All three of these DBHS proteins contain conserved tandem motifs and often co-localize and co-purify together.[5] To investigate whether NONO and PSPC1 modulate innate immune responses, we depleted NONO or PSPC1 in HUVEC cells to determine their impact on innate immune signaling pathways. Our data showed that only SFPQ, but not the other DBHS proteins, could prevent the induction of the type I IFN response in HUVEC cells (Figure S10).

MDA5 contributes to the type I IFN response induced by SFPQ deficiency in uninfected cells

To test whether the increased levels of MDA5 (also known as IFIH1) mRNA and protein in SFPQ-depleted cells (Figures 4B and 4H) were required for the induction of the innate immune response, we knocked down MDA5 or its adaptor protein MAVS in SFPQ-deficient HUVEC cells. As described above, the mRNA levels of ISGs were increased in SFPQ-deficient HUVEC cells. This increase was abolished in cells co-transfected with MDA5 and SFPQ siRNA, or MAVS and SFPQ siRNA (Figures 5A-5H). Silencing of MDA5 or MAVS in SFPQ-depleted cells significantly decreased phosphorylation of IRF3, as well as the protein expression of IFIT1 and IFIT3, compared to cells transfected with SFPQ alone (Figures 5D and S11A). The knockdown efficiency was confirmed by western blot or RT-qPCR (Figures 5D and S11B).

To examine whether MDA5 activation depends on host RNAs in SFPQ-deficient cells. We treated uninfected HUVEC cells with α-amanitin or actinomycin-D (ActD). α-amanitin inhibits RNA polymerase II and possibly also pol III activation.[32,33] ActD suppresses *de novo* RNA synthesis.[34,35] Hence, we hypothesized that either drug would counteract SFPQ-mediated induction of MDA5. The cells were treated with IFNβ for a total of 24 h. After the initial 12 h of IFNβ treatment, the cells were co-incubated with actinomycin D or α-amanitin for the remaining 12 h. Depletion of SFPQ significantly induced the expression of MDA5 compared to control cells, and the induction was further elevated after adding IFNβ. However, treatment of SFPQ-depleted cells with α-amanitin or ActD significantly decreased the induction of MDA5, ZBP1, and other ISG proteins in both mock and IFNβ--treated cells (Figures 5I and S11C). The mRNA expression of β-actin indicated that neither α-amanitin nor ActD blocked global transcription (Figure S11D).

To determine which domain of SFPQ contributes to the suppression of the type I IFN response, SFPQ-KO cells were reconstituted with either full-length SFPQ or SFPQ truncations and then tested for their ability to reverse the induction of ISGs. Briefly, we generated full-length SFPQ or SFPQ truncations containing a PAM site mutant to abolish Cas9 nuclease activity. We transfected NTC or sgRNA targeting SFPQ in HUVEC^{cas9} cells and then transfected them with an empty vector (EV), full-length SFPQ, or SFPQ truncations (Figure 5J). As before, SFPQ knockout increased the expression of MDA5 and pIRF3 compared to NTC control cells when both were transfected with EV. However, SFPQ-KO cells transfected with full-length SFPQ abolished MDA5 and pIRF3 induction compared to EV-transfected SFPQ-KO cells. Induction of MDA5 and pIRF3 was also reduced in SFPQ-ΔDBD- or SFPQ-ΔRRM1-expressing SFPQ-KO cells, but not in SFPQ-KO cells reconstituted with the SFPQ-ΔRRM2 truncation (Figure 5K). This indicates that the RRM2 domain of SFPQ is important for suppressing MDA5 and the innate immune response.

SFPQ preserves cell viability

We observed a defect in cell growth in SFPQ-deficient cells compared to control cells (Figures S12A-S12C). Knockout of SFPQ led to the activation of ZBP1 and MDA5, both of which have been reported to mediate cell death in ADAR1-deficient cells (Figures 4H and S4).[36] To investigate whether the cell growth inhibition caused by SFPQ depletion is related to MDA5 and ZBP1, we examined their interplay. Given that ZBP1 expression is induced by IFNβ and MDA5 promotes IFNβ production in SFPQ-depleted cells (Figures 4 and 6A-6D), we hypothesized that MDA5 loss might suppress ZBP1 expression by reducing IFN signaling. Consistent with this, the knockdown of MDA5 in SFPQ-depleted cells led to a reduction in ZBP1 expression compared to SFPQ knockdown alone, but it did not completely prevent ZBP1 upregulation (Figures 6C and 6E). Moreover, MDA5 and SFPQ double knockdown partially rescued the cell viability defects observed with SFPQ knockdown alone (Figures 6F, 6G, and S11E).

To further explore the role of ZBP1 in regulating cell growth in SFPQ-depleted cells, we depleted SFPQ in EA.hy926 endothelial cells and observed induction of ZBP1 and its downstream target pRIP3 (Figure 6H). As expected, SFPQ knockout significantly inhibited

cell growth in these cells (Figure 6I). However, co-depletion of ZBP1 and SFPQ (Figures 6J-6N) led to an increase in cell viability compared to SFPQ knockdown alone, indicating that ZBP1 contributes to cell arrest following SFPQ depletion (Figures 6M and 6N). Furthermore, triple knockdown of SFPQ, ZBP1, and MDA5 (Figures 6J-6M) resulted in an even greater rescue of cell growth (Figures 6M and 6N). Together, our data suggest that SFPQ preserves cell viability, at least in part, by repressing the expression of MDA5 and ZBP1.

DISCUSSION

SFPQ plays a pivotal role in RNA metabolism, as it has the ability to interact with nucleic acids, influencing various processes such as RNA transcriptional regulation,[37] non-coding RNA stability, circRNA biogenesis,[7] pre-mRNA splicing, and 3′ UTR processing.[38] In addition to SFPQ's role in modulating the transcription and replication of certain RNA viruses,[13,14] it has also been reported to affect Epstein-Barr virus (EBV) gene expression, repress the EBV latent to lytic transition,[39] and promote KSHV DNA replication.[40]

Here, we report a new role for SFPQ in preventing cellular RNA from triggering innate immune responses in both uninfected and virus-infected cells. During KSHV lytic reactivation, type I IFN was augmented in SFPQ-depleted cells compared to latently infected cells. This IFN response inhibited viral replication, which was partially restored by concurrently depleting both IRF3 and SFPQ. The loss of SFPQ activated the dsRNA sensor, MDA5, and induced innate immune responses. In contrast, this response was abolished in cells depleted for both MDA5 and SFPQ or when cellular RNA synthesis was inhibited.

ADAR1 is a key player in preventing endogenous RNAs from triggering an innate immune response. SFPQ associates with ADAR1 in an RNA-dependent manner, and the nucleic acid-binding domain of SFPQ was essential for the SFPQ-ADAR1 association and modulation of the IFN response. Given that SFPQ is a multifunctional protein capable of binding both DNA and RNA, it is possible that the RRM2 domain is the major domain required for both functions- associated with ADAR1- and IFNb-dependent signaling. We speculate that the DBD domain may alter the overall protein conformation of SFPQ to stabilize its association with ADAR1, but the RRM2 domain may be the critical domain involved in the modulation of IFN signaling. There is an A-to-I editing site in the NEAT1 transcript catalyzed by ADAR1 that has previously been reported.[29] Additionally, we identified four A-to-I editing sites in the transcripts of ARHGAP26, SNRPD3, SDHAF4, and ZNF488, all of which were also edited by ADAR1. Notably, the editing sites in ARHGAP26[30] and SNRPD3[31] transcripts had been previously predicted by RNA-seq analysis, while A-to-I editing of SDHAF4 and ZNF488 is reported in this study. We found that the loss of SFPQ decreased the A-to-I editing frequency of these five RNA transcripts. Therefore, we suggest that SFPQ facilitates ADAR1 A-to-I editing efficiency, thereby shielding cellular RNAs from the dsRNA sensor, MDA5, and blunting MDA5-mediated innate immune responses.

In addition to regulating MDA5 activation, SFPQ depletion induced the expression of the ISG, ZBP1. ZBP1 expression was further increased with IFNβ treatment in SFPQ-depleted

cells. ZBP1 interacts with RIPK3 via RHIM-RHIM homotypic interactions, thereby activating inflammatory cell death, PANoptosis.[41] Our results show that SFPQ depletion increased RIPK3 phosphorylation and that the knockdown of ZBP1 in SFPQ-depleted cells partially rescued cell death. Therefore, although ZBP1 is not the primary driver of SFPQ depletion-induced cell death, it does contribute to the cell death phenotype observed in SFPQ-deficient cells. When MDA5 or MAVS was depleted in SFPQ knockdown cells, activation of type I IFN and ISG was diminished. ZBP1 mRNA levels were also decreased when MDA5 or MAVS was depleted in SFPQ knockdown cells but nevertheless remained higher than that in the NTC control cells. This suggests that SFPQ modulates ZBP1 in a manner that is not solely dependent on the MDA5-mediated IFN response. ZBP1 was originally identified as a DNA sensor and is now known to also sense RNA that might exist in the Z conformation. ADAR1 and ZBP1 are the only identified proteins that contain a Z-DNA/RNA binding domain and can bind Z-form DNA/RNA. ADAR1 is necessary to prevent ZBP1 activation, which is dependent on Z-RNA.[42] There is no obvious Z-RNA binding domain in SFPQ, although we found that the RNA-binding ability of SFPQ was required for the association with ADAR1.

In summary, we report a role for SFPQ in binding ADAR1 and modulating its editing function in both virus-infected and uninfected cells. By doing so, SFPQ inhibits cellular RNAs from activating MDA5-mediated innate immune responses and also preserves cell viability.

Limitations of the study

The level of RNA editing is a highly regulated process influenced by multiple factors. Several proteins have been shown to modulate ADAR1 editing function by affecting RNA secondary structure, RNA substrate accessibility, and the positioning of ADAR1 on target transcripts. While we provide evidence that SFPQ can inhibit the innate immune response in both uninfected and virus-infected cells by associating with ADAR1 and modulating its A-to-I editing function, there is no obvious Z-RNA binding domain in SFPQ. Hence, this suggests that SFPQ's interaction with ADAR1 alters its activity but not by directly binding the Z-RNA portion of its substrate, although it may be able to bind non-Z-RNA portions of the same RNA transcript since the SFPQ-ADAR1 interaction appears to be RNA-dependent. We confirmed that SFPQ modulates ADAR1 editing of five RNA transcripts, and a future goal is to confirm editing of other transcripts whose editing appears to change in the presence versus absence of SFPQ.

STAR★METHODS

EXPERIMENTAL MODEL AND STUDY PARTICIPANT DETAILS

Cell lines: HUVEC were maintained in EGM-2 supplied with growth factors from the EGM-2 Bullet kit (Lonza). iSLK.219 cells (a kind gift from Dr. Don Ganem) were maintained in DMEM medium (Corning) containing 10% tetracycline (Tet)-free FBS (Sigma), 1% pen-strep (Corning), 10 μg/mL puromycin (Corning), 250 μg/mL geneticin (Corning), and 400 μg/mL hygromycin B (Corning). BCBL1-TREx-RTA cells (a kind gift from Dr. Jae Jung) were cultured in RPMI 1640 (Corning) medium supplemented with

10% tetracycline (Tet)-free FBS, 1% pen-strep, 1% L-glutamine, 1% sodium bicarbonate, 0.05 mM β-mercaptoethanol, and 20 μg/mL hygromycin. HEK293T and 293FT cells were maintained in DMEM medium containing 10% FBS and 1% pen-strep. All cells were kept at 37°C in a 5% CO_2 incubator. Commercially obtained cells were authenticated by the vendors (ATCC and Thermo Fisher) and not revalidated by our laboratory. All cell lines were routinely tested for mycoplasma contamination by PCR.

iSLK.219^{cas9} and HUVEC^{cas9} cell generation: Lentiviral cas9 nuclease expression vector containing a human codon-optimized version of the *S. pyogenes* Cas9 nuclease was purchased from Dharmacon. Lentiviral particles were produced using the ViraPower Lentiviral Expression System (Invitrogen) in 293FT cells according to the manufacturer's protocol. The supernatant containing viral particles was harvested and used to infect iSLK.219 and HUVEC cells. Infected cells were selected with 7 μg/mL blasticidin (Invitrogen) for a week. The Cas9-expressing cells were then transfected with SFPQ sgRNA or non-targeting control sgRNA (Dharmacon, sgRNA sequences are listed in Table S2) with Lipofectamine RNAiMax (Invitrogen) at the indicated times for later analysis.

METHOD DETAILS

siRNA, viral reactivation, and fluorescence microscopy: iSLK.219 and HUVEC cells were transfected with the indicated siRNAs (Dharmacon, siRNA sequences are listed in Table S2) using Lipofectamine RNAiMax (Invitrogen). iSLK.219 cells were replenished with complete DMEM medium containing 0.2 μg/mL Dox at 48 h post-transfection. The cells were collected at the indicated time for later analysis. GFP and RFP images were taken with a Leica DMi8 microscope with the same exposure time setting. The RFP/GFP fluorescence intensity of images was analyzed with a CLARIOstar plate reader.

shRNA and KSHV reactivation: The non-target shRNA control and two shRNAs targeting SFPQ in the pLKO.5-puro background were purchased from Sigma Aldrich. Lentivirus for each of the shRNAs was produced with the ViraPower Lentiviral Expression System (Invitrogen) in 293FT cells according to the manufacturer's instructions. The supernatant containing viral particles was harvested and used to infect BCBL1-TRex-RTA using 4 μg/mL polybrene. Infected cells were selected with 1 μg/mL puromycin for 3 days, and then the medium was changed to complete RPMI 1640 containing 0.1 μg/mL doxycycline for KSHV reactivation. Cells were collected at the indicated time for later analysis.

Plasmid construction and transfection: A full-length HA-SFPQ ORF expression vector was obtained from Dr. Rosalind Segal through Addgene (plasmid,166959). The plasmids were transfected into HEK293T cells using Lipofectamine 2000 (Invitrogen) and then harvested at 48 h post-transfection for the immunoprecipitation assay. SFPQ-truncated mutant plasmids were PCR amplified from full-length SFPQ with the Q5 Site-Directed Mutagenesis Kit (NEB, E0554S) using the indicated primers (sequences are listed in Table S3). HUVEC-Cas9-expressing cells were transfected with SFPQ sgRNA or non-targeting control. Twenty-four hours after sgRNA treatment, the cells were transfected with the empty plasmid, full-length SFPQ, or truncated mutant SFPQ plasmids using Human

Umbilical Vein Endothelial Cell Nucleofector Kit (Lonza) according to the manufacturer's recommendations. Cells were collected after 48 h for late analysis.

Immunoblotting, immunoprecipitation, and ELISA: Whole-cell lysates were prepared in SDS-sample loading buffer (60mM Tris-HCl, pH 6.8, 2% SDS, 10% glycerol, 5% β-mercaptoethanol, 0.01% bromophenol blue), separated by SDS-PAGE, and then transferred to nitrocellulose membranes (GE Healthcare). The membrane was blocked in TBS-T (TBS with 0.5% Tween 20) with 5% nonfat milk (Apex) and then incubated with the indicated primary antibody at 4°C overnight. IFNβ and CXCL10/IP-10 proteins in the supernatant were quantified using the Human IFN-beta DuoSet ELISA kit (R&D Systems) and Human CXCL10/IP-10 ELISA kit (Abcam), respectively. Protein levels (pg/mL) were calculated based on the standard curve generated in the assays.

For immunoprecipitation assays, HEK293T cells transfected with SFPQ FL or SFPQ mutants were lysed using 500 μL of IP buffer (Thermo Fisher) with complete protease inhibitor cocktail and centrifuged to remove cell debris. The lysates were incubated with anti-HA magnetic beads (Thermo Fisher) overnight at 4°C. Two million HEK293T cells were lysed with 500 μL IP buffer and centrifuged to remove cell debris. The cell lysates were incubated with 1 μg of SFPQ, ADAR1, or IgG antibody overnight at 4°C and coupled to Protein G Dynabeads (Thermo Fisher) for 1 h. To examine RNA-dependent interactions, RNase A was added to cell lysates and incubated at 37°C for 1 h. The beads were washed four times with IP buffer for 5 min each. Elution from the beads was performed in 2× sample loading buffer by incubating at 95°C for 5 min. The protein samples were then analyzed by western blot.

Immunofluorescence microscopy: iSLK.219 cells were treated with Dox or DMSO for 64 h and then fixed with 4% formaldehyde in PBS at room temperature for 10 min and permeabilized with 0.1% Triton X- and 1% BSA in PBS for 30 min at room temperature. Primary antibodies against SFPQ (Abcam) or ADAR1 were diluted in PBS with 0.1% Triton X- and 1% BSA, then incubated with the fixed cells overnight at 4°C. A fluorescently labeled secondary antibody was used to reveal SFPQ or ADAR1 proteins. Images were collected using a Leica DMi8 microscope.

Cell growth assay: Viable cells were identified by Trypan Blue exclusion (Thermo Fisher) and counted with a hemocytometer. The live cells were stained with calcein green dye (Thermo Fisher). Images were collected with a Leica DMi8 microscope, and the fluorescent signal was measured by plate reader. The MTT assay (Abcam) was also used to assess viable cells according to the manufacturer's instructions.

VSV infection: HUVEC were transfected with NTC and SFPQ siRNA for two days and then inoculated with VSV (MOI = 1) for 1 h in basal DMEM medium. The virus-containing supernatant was subsequently removed and replaced with DMEM medium supplemented with 2% FBS for another 24 h. Supernatant from the infected cells was subjected to a serial dilution in basal DMEM medium and used to infect Vero cells for 1 h. The supernatant was then removed and replaced with a DMEM overlay containing 2% FBS and 0.5% methylcellulose. Plaques were allowed to develop for 24 h at 37°C before being fixed and

stained in a solution containing 0.1% crystal violet and 30% methanol for 10 m. Plaques were counted using a dissecting microscope and viral titers were calculated and presented in PFU per milliliter using the following formula: PFU/mL = # of plaques/(dilution factor x volume plated in milliliter).

RNA sequencing and bioinformatics analysis: iSLK.219 cells were transfected with NTC or SFPQ siRNA for 48 h, after which the cells were collected. Total RNAs were extracted with the RNeasy Plus Mini Kit (QIAGEN) and sent to Azenta Life Sciences for RNA-seq library preparation and analysis. Sequence reads were mapped to the human reference genome (30–680281665_GRCh38) and KSHV reference genome (OK358814.1) using the STAR aligner v.2.5.2b. The sequences were analyzed using featureCounts from the Subread package v.1.5.2 (Azenta) and CLC Genomics Workbench 23 (Qiagen). The variants (SNP, Single Nucleotide Polymorphism) were detected using Varscan v2.3.9 (Azenta).

Quantitative real-time PCR and PCR arrays: Total RNA was extracted with RNeasy Plus Mini Kit (QIAGEN), and cDNA synthesis was performed using a SensiFAST cDNA Synthesis Kit (Bioline). Real-time qPCR was conducted using Sensi-Fast SYBR (Bioline), with normalization to the housekeeping gene ACTB. All primer sequences are listed in Table S3. For PCR array, total RNA was extracted from HUVEC cells, and cDNA synthesis was performed as described aforementioned. Human Type I Interferon Response PCR Array from QIAGEN, containing 84 primer sets against human interferon signaling-related genes, was utilized. Real-time PCR was carried out according to the manufacturer's protocol, and ISG expression was normalized to housekeeping genes.

Sanger sequencing: HUVEC-Cas9 cells were transfected with NTC or SFPQ sgRNA for 72 h, after which cells were collected. Total RNA was extracted using a RNeasy Plus Mini Kit (QIAGEN), and cDNA was synthesized with SensiFAST cDNA Synthesis Kit (Bioline). Gene-specific amplification was performed with Q5 High-Fidelity DNA polymerase (NEB), following the manufacturer's guidelines. The primer sequences used for amplifying are listed in Table S3. PCR products were purified and sequenced by Eurofins Genomics.

Statistical analysis: For all figures, data are shown as mean ± SD. Statistical significance of differences in mRNA expression level, MTT, and CXCL10 concentration were determined using Student's *t* test (two-tailed). For all tests, a *p* value of <0.05 was considered statistically significant. * indicates $p < 0.05$.

Supplementary Material

Refer to Web version on PubMed Central for supplementary material.

ACKNOWLEDGMENTS

We thank Dr. Jae Jung for the gift of the TREx BCBL1-RTA cells and Dr. Don Ganem for the iSLK.219 cells. We thank Patricio Cano for helpful advice and Whitney Tevebaugh for proofreading. The graphical abstract was created using Biorender. We would also like to acknowledge our funding sources, NCI/NIH CA019014, CA291437, CA294800, and CA163217.

REFERENCES

1. McNab F, Mayer-Barber K, Sher A, Wack A, and O'Garra A (2015). Type I interferons in infectious disease. Nat. Rev. Immunol 15, 87–103. 10.1038/nri3787. [PubMed: 25614319]
2. Rehwinkel J, and Gack MU (2020). RIG-I-like receptors: their regulation and roles in RNA sensing. Nat. Rev. Immunol 20, 537–551. 10.1038/s41577-020-0288-3. [PubMed: 32203325]
3. Ivashkiv LB, and Donlin LT (2014). Regulation of type I interferon responses. Nat. Rev. Immunol 14, 36–49. 10.1038/nri3581. [PubMed: 24362405]
4. Yarosh CA, Iacona JR, Lutz CS, and Lynch KW (2015). PSF: nuclear busy-body or nuclear facilitator? Wiley Interdiscip. Rev. RNA 6, 351–367. 10.1002/wrna.1280. [PubMed: 25832716]
5. Lim YW, James D, Huang J, and Lee M (2020). The Emerging Role of the RNA-Binding Protein SFPQ in Neuronal Function and Neurodegeneration. Int. J. Mol. Sci 21, 7151. 10.3390/ijms21197151. [PubMed: 32998269]
6. Emili A, Shales M, McCracken S, Xie W, Tucker PW, Kobayashi R, Blencowe BJ, and Ingles CJ (2002). Splicing and transcription-associated proteins PSF and p54nrb/nonO bind to the RNA polymerase II CTD. RNA 8, 1102–1111. 10.1017/s1355838202025037. [PubMed: 12358429]
7. Stagsted LVW, O'Leary ET, Ebbesen KK, and Hansen TB (2021). The RNA-binding protein SFPQ preserves long-intron splicing and regulates circRNA biogenesis in mammals. eLife 10, 63088. 10.7554/eLife.63088.
8. Gordon PM, Hamid F, Makeyev EV, and Houart C (2021). A conserved role for the ALS-linked splicing factor SFPQ in repression of pathogenic cryptic last exons. Nat. Commun 12, 1918. 10.1038/s41467-021-22098-z. [PubMed: 33771997]
9. Zhang Z, and Carmichael GG (2001). The fate of dsRNA in the nucleus: a p54(nrb)-containing complex mediates the nuclear retention of promiscuously A-to-I edited RNAs. Cell 106, 465–475. 10.1016/s0092-8674(01)00466-4. [PubMed: 11525732]
10. Kanai Y, Dohmae N, and Hirokawa N (2004). Kinesin transports RNA: isolation and characterization of an RNA-transporting granule. Neuron 43, 513–525. 10.1016/j.neuron.2004.07.022. [PubMed: 15312650]
11. Zhou B, Qi F, Wu F, Nie H, Song Y, Shao L, Han J, Wu Z, Saiyin H, Wei G, et al. (2019). Endogenous Retrovirus-Derived Long Noncoding RNA Enhances Innate Immune Responses via Derepressing RELA Expression. mBio 10, e00937.19. 10.1128/mBio.00937-19. [PubMed: 31363026]
12. Imamura K, Imamachi N, Akizuki G, Kumakura M, Kawaguchi A, Nagata K, Kato A, Kawaguchi Y, Sato H, Yoneda M, et al. (2014). Long noncoding RNA NEAT1-dependent SFPQ relocation from promoter region to paraspeckle mediates IL8 expression upon immune stimuli. Mol. Cell 53, 393–406. 10.1016/j.molcel.2014.01.009. [PubMed: 24507715]
13. Landeras-Bueno S, Jorba N, Pérez-Cidoncha M, and Ortín J (2011). The splicing factor proline-glutamine rich (SFPQ/PSF) is involved in influenza virus transcription. PLoS Pathog. 7, e1002397. 10.1371/journal.ppat.1002397. [PubMed: 22114566]
14. Flather D, Nguyen JHC, Semler BL, and Gershon PD (2018). Exploitation of nuclear functions by human rhinovirus, a cytoplasmic RNA virus. PLoS Pathog. 14, e1007277. 10.1371/journal.ppat.1007277. [PubMed: 30142213]
15. Wong JP, and Damania B (2017). Modulation of oncogenic signaling networks by Kaposi's sarcoma-associated herpesvirus. Biol. Chem 398, 911–918. 10.1515/hsz-2017-0101. [PubMed: 28284028]
16. Belur NR, Bustos BI, Lubbe SJ, and Mazzulli JR (2024). Nuclear aggregates of NONO/SFPQ and A-to-I-edited RNA in Parkinson's disease and dementia with Lewy bodies. Neuron 112, 2558–2580.e13. 10.1016/j.neuron.2024.05.003. [PubMed: 38761794]
17. Zhang H, Sandhu PK, and Damania B (2023). The Role of RNA Sensors in Regulating Innate Immunity to Gammaherpesviral Infections. Cells 12, 1650. 10.3390/cells12121650. [PubMed: 37371120]
18. West JA, Wicks M, Gregory SM, Chugh P, Jacobs SR, Zhang Z, Host KM, Dittmer DP, and Damania BJ (2014). An important role for mitochondrial antiviral signaling protein in the Kaposi's sarcoma-associated herpesvirus life cycle. Virol 88, 5778–5787. 10.1128/JVI.03226-13.

19. Zhang Y, Dittmer DP, Mieczkowski PA, Host KM, Fusco WG, Duncan JA, and Damania B (2018). RIG-I Detects Kaposi's Sarcoma-Associated Herpesvirus Transcripts in a RNA Polymerase III-Independent Manner. mBio 9, e00823–18. 10.1128/mBio.00823-18. [PubMed: 29970461]
20. Zhao Y, Ye X, Dunker W, Song Y, and Karijolich J (2018). RIG-I like receptor sensing of host RNAs facilitates the cell-intrinsic immune response to KSHV infection. Nat. Commun 9, 4841. 10.1038/s41467-018-07314-7. [PubMed: 30451863]
21. Zhang H, Ni G, and Damania B (2020). ADAR1 Facilitates KSHV Lytic Reactivation by Modulating the RLR-Dependent Signaling Pathway. Cell Rep. 31, 107564. 10.1016/j.celrep.2020.107564. [PubMed: 32348766]
22. Myoung J, and Ganem D (2011). Generation of a doxycycline-inducible KSHV producer cell line of endothelial origin: maintenance of tight latency with efficient reactivation upon induction. J. Virol. Methods 174, 12–21. 10.1016/j.jviromet.2011.03.012. [PubMed: 21419799]
23. Sun R, Lin S-F, Gradoville L, Yuan Y, Zhu F, and Miller G (1998). A viral gene that activates lytic cycle expression of Kaposi's sarcoma-associated herpesvirus. Proc. Natl. Acad. Sci. USA 95, 10866–10871. [PubMed: 9724796]
24. Nakamura H, Lu M, Gwack Y, Souvlis J, Zeichner SL, and Jung JU (2003). Global changes in Kaposi's sarcoma-associated virus gene expression patterns following expression of a tetracycline-inducible Rta transactivator. J. Virol 77, 4205–4220. 10.1128/jvi.77.7.4205-4220.2003. [PubMed: 12634378]
25. Wu J, and Chen ZJ (2014). Innate immune sensing and signaling of cytosolic nucleic acids. Annu. Rev. Immunol 32, 461–488. 10.1146/annurev-immunol-032713-120156. [PubMed: 24655297]
26. Fitzgerald KA, McWhirter SM, Faia KL, Rowe DC, Latz E, Golenbock DT, Coyle AJ, Liao SM, and Maniatis T (2003). IKKepsilon and TBK1 are essential components of the IRF3 signaling pathway. Nat. Immunol 4, 491–496. 10.1038/ni921. [PubMed: 12692549]
27. Patterson JB, and Samuel CE (1995). Expression and regulation by interferon of a double-stranded-RNA-specific adenosine deaminase from human cells: evidence for two forms of the deaminase. Mol. Cell Biol 15, 5376–5388. 10.1128/MCB.15.10.5376. [PubMed: 7565688]
28. Lee M, Sadowska A, Bekere I, Ho D, Gully BS, Lu Y, Iyer KS, Trewhella J, Fox AH, and Bond CS (2015). The structure of human SFPQ reveals a coiled-coil mediated polymer essential for functional aggregation in gene regulation. Nucleic Acids Res. 43, 3826–3840. 10.1093/nar/gkv156. [PubMed: 25765647]
29. Vlachogiannis NI, Sachse M, Georgiopoulos G, Zormpas E, Bampatsias D, Delialis D, Bonini F, Galyfos G, Sigala F, Stamatelopoulos K, et al. (2021). Adenosine-to-inosine Alu RNA editing controls the stability of the pro-inflammatory long noncoding RNA NEAT1 in atherosclerotic cardiovascular disease. J. Mol. Cell. Cardiol 160, 111–120. 10.1016/j.yjmcc.2021.07.005. [PubMed: 34302813]
30. Wang Q, Hui H, Guo Z, Zhang W, Hu Y, He T, Tai Y, Peng P, and Wang L (2013). ADAR1 regulates ARHGAP26 gene expression through RNA editing by disrupting miR-30b-3p and miR-573 binding. RNA 19, 1525–1536. 10.1261/rna.041533.113. [PubMed: 24067935]
31. Wei Q, Han S, Yuan K, He Z, Chen Y, Xi X, Han J, Yan S, Chen Y, Yuan B, et al. (2023). Transcriptome-wide profiling of A-to-I RNA editing by Slic-seq. Nucleic Acids Res. 51, e87. 10.1093/nar/gkad604. [PubMed: 37470992]
32. Lindell TJ, Weinberg F, Morris PW, Roeder RG, and Rutter WJ (1970). Specific inhibition of nuclear RNA polymerase II by alpha-amanitin. Science 170, 447–449. 10.1126/science.170.3956.447. [PubMed: 4918258]
33. Weinmann R, and Roeder RG (1974). Role of DNA-dependent RNA polymerase 3 in the transcription of the tRNA and 5S RNA genes. Proc. Natl. Acad. Sci. USA 71, 1790–1794. 10.1073/pnas.71.5.1790. [PubMed: 4525293]
34. Sobell HM (1985). Actinomycin and DNA transcription. Proc. Natl. Acad. Sci. USA 82, 5328–5331. 10.1073/pnas.82.16.5328. [PubMed: 2410919]
35. Perry RP, and Kelley DE (1970). Inhibition of RNA synthesis by actinomycin D: characteristic dose-response of different RNA species. J. Cell. Physiol 76, 127–139. 10.1002/jcp.1040760202. [PubMed: 5500970]

36. Liddicoat BJ, Piskol R, Chalk AM, Ramaswami G, Higuchi M, Hartner JC, Li JB, Seeburg PH, and Walkley CR (2015). RNA editing by ADAR1 prevents MDA5 sensing of endogenous dsRNA as nonself. Science 349, 1115–1120. 10.1126/science.aac7049. [PubMed: 26275108]

37. Takeuchi A, Iida K, Tsubota T, Hosokawa M, Denawa M, Brown JB, Ninomiya K, Ito M, Kimura H, Abe T, et al. (2018). Loss of Sfpq Causes Long-Gene Transcriptopathy in the Brain. Cell Rep. 23, 1326–1341. 10.1016/j.celrep.2018.03.141. [PubMed: 29719248]

38. Rosonina E, Ip JYY, Calarco JA, Bakowski MA, Emili A, McCracken S, Tucker P, Ingles CJ, and Blencowe BJ (2005). Role for PSF in mediating transcriptional activator-dependent stimulation of pre-mRNA processing in vivo. Mol. Cell Biol 25, 6734–6746. 10.1128/MCB.25.15.6734-6746.2005. [PubMed: 16024807]

39. Murray-Nerger LA, Lozano C, Burton EM, Liao Y, Ungerleider NA, Guo R, and Gewurz BE (2024). The nucleic acid binding protein SFPQ represses EBV lytic reactivation by promoting histone H1 expression. Nat. Commun 15, 4156. 10.1038/s41467-024-48333-x. [PubMed: 38755141]

40. Payen SH, Andrada K, Tara E, Petereit J, Verma SC, and Rossetto CC (2024). The cellular paraspeckle component SFPQ associates with the viral processivity factor ORF59 during lytic replication of Kaposi's Sarcoma-associated herpesvirus (KSHV). Virus Res. 349, 199456. 10.1016/j.virusres.2024.199456. [PubMed: 39214388]

41. Kuriakose T, Man SM, Malireddi RKS, Karki R, Kesavardhana S, Place DE, Neale G, Vogel P, and Kanneganti TD (2016). ZBP1/DAI is an innate sensor of influenza virus triggering the NLRP3 inflammasome and programmed cell death pathways. Sci. Immunol 1, aag2045. 10.1126/sciimmunol.aag2045. [PubMed: 27917412]

42. Zhang Y, Zhang J, and Xue Y (2023). ADAR1: a mast regulator of aging and immunity. Signal Transduct. Target. Ther 8, 7. 10.1038/s41392-022-01276-5. [PubMed: 36596768]

Highlights

- SFPQ modulates the type I interferon response in MDA5-dependent manner
- SFPQ acts as a proviral factor for KSHV lytic reactivation
- SFPQ associates with ADAR1 and modulates A-to-I editing of cellular RNA transcripts
- SFPQ preserves endothelial cell viability

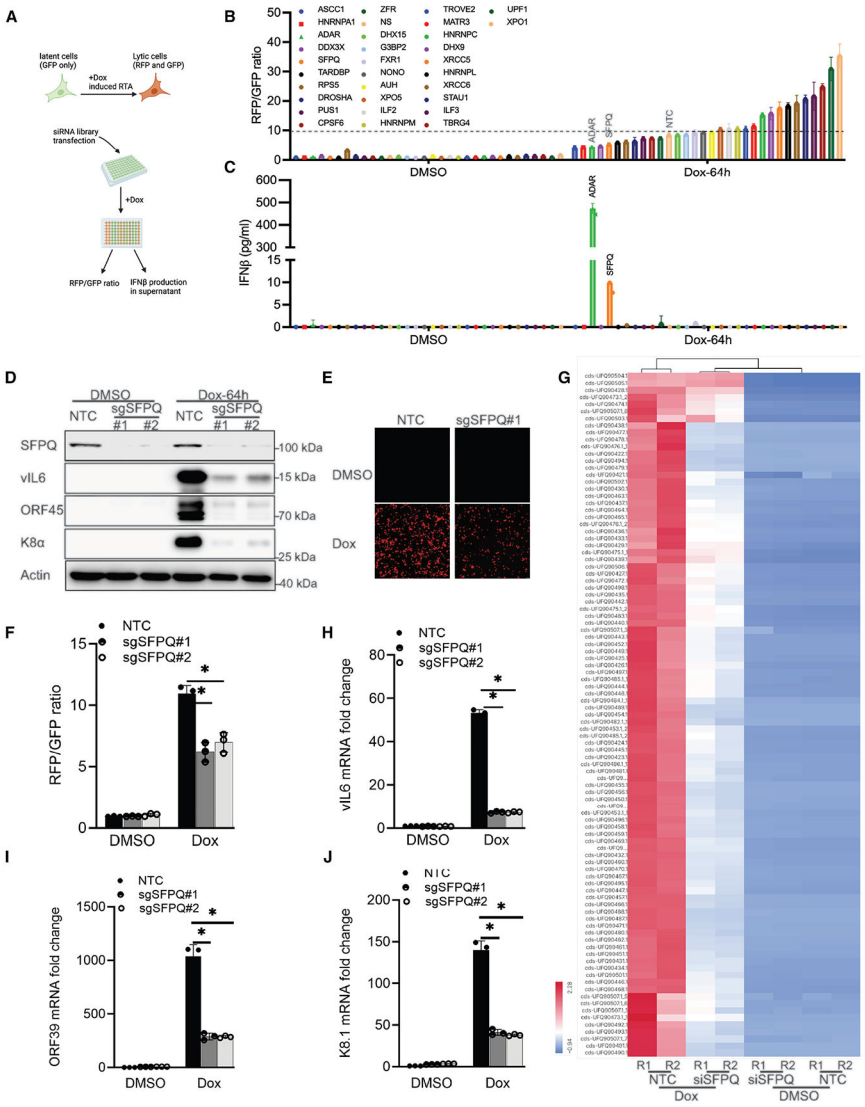

Figure 1. Depletion of SFPQ reduces viral replication during RTA-induced KSHV lytic reactivation

(A–C) Analysis of RFP/GFP intensity and IFN production upon siRNA knockdown of RBPs during KSHV lytic reactivation. iSLK.219 cells were transfected with non-specific control (NTC) siRNAs or siRNAs targeting RBPs for 48 h and then treated with DMSO or 0.2 μg/mL Dox for 64 h. Schematic of the RBP-targeted siRNA screening in iSLK.219 cells during KSHV lytic reactivation. GFP and RFP intensities were measured by a CLARIOstar plate reader, and the RFP/GFP ratio was calculated from DMSO- and Dox-treated cells (A and B). IFNβ production in the supernatant was measured by ELISA (C).

(D–F) iSLK.219 cells constitutively expressing Cas9 were transfected with non-targeting control (NTC) or two different sgRNAs targeting SFPQ and then treated with DMSO or 0.2 μg/mL Dox. The protein expression of SFPQ and viral genes was measured by western blot. RFP-positive cells were imaged. Scale bars, 100 μm (D). The RFP/GFP ratio was calculated from DMSO- and Dox-treated cells (E and F).

(G) iSLK.219 cells were treated the same as (A)–(C). RNA was extracted from the cells and subjected to RNA-seq analysis. The heatmap displays the global KSHV viral transcripts from RNA-seq data. Red indicates high gene expression, while light blue indicates low gene expression, and dark blue indicates no gene expression.

(H–J) Cells were treated the same as in (D). The mRNA expression levels of KSHV genes were measured by real-time PCR.

(A)–(C) and (G) are representative of two independent experiments. The data in (D)–(F) and (H)–(J) are representative of three independent experiments. The bar charts are presented as mean ± SD. *$p < 0.05$ by Student's *t* test.

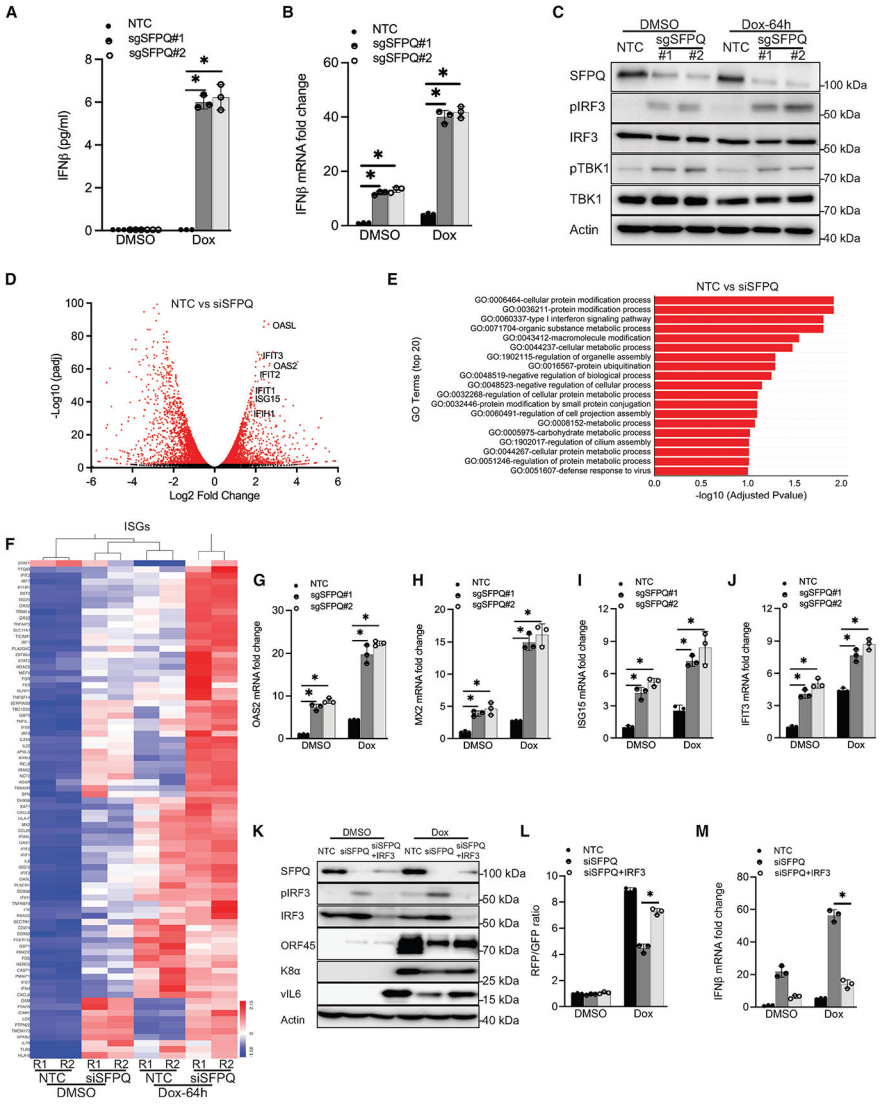

Figure 2. Depletion of SFPQ induces type I IFN signaling in latent and lytic KSHV-infected cells

(A) The protein expression level of IFNβ in the supernatant was measured by ELISA.

(B) The mRNA expression level of IFNβ gene was measured by real-time PCR.

(C) Cell lysates were collected, and western blots were performed with the indicated antibodies. For total IRF3 levels, the western blot for phospho-IRF3 was stripped and reprobed with an antibody against total IRF3.

(D–F) RNA-seq data from Figure 1 was analyzed for IFN pathway genes. Volcano plot (D) visualizing the cellular transcriptional change in RNA-seq data. Gene Ontology analysis (E) of significantly differentially expressed genes enrichment from RNA-seq data. Heatmap (F) displaying expression of interferon-stimulated genes (ISGs) from RNA-seq data.

(G–J) RNA extracted from iSLK.219-Cas9 cells treated with NTC and SFPQ sgRNA as described previously. The mRNA expression levels of OAS2 (G), MX2 (H), ISG15 (I), and IFIT3 (J) were measured by real-time PCR.

(K)–(M) iSLK.219 cells were transfected with SFPQ siRNA alone or together with IRF3 siRNA for 48 h and then reactivated with Dox (0.2 μg/mL) for 0 and 64 h. Cells were

harvested at different time points, and western blots were performed with the indicated antibodies (K). For total IRF3 levels, the western blot for phospho- IRF3 was stripped and reprobed with an antibody against total IRF3. GFP and RFP intensities were measured by a CLARIOstar plate reader, and the ratio of RFP/GFP was calculated for the indicated times (L). The mRNA and protein expression of IFNβ was measured by real-time PCR (M). iSLK.219-Cas9 cells were transfected with a non-targeting sgRNA or two different sgRNAs targeting SFPQ for 48 h and then treated with 0.2 μg/mL Dox for 64 h. The data in (A)–(C) and (G)–(M) are representative of three independent experiments. The data in (D)–(F) are representative of two independent experiments. The bar charts are presented as mean ± SD. *$p < 0.05$ by Student's *t* test.

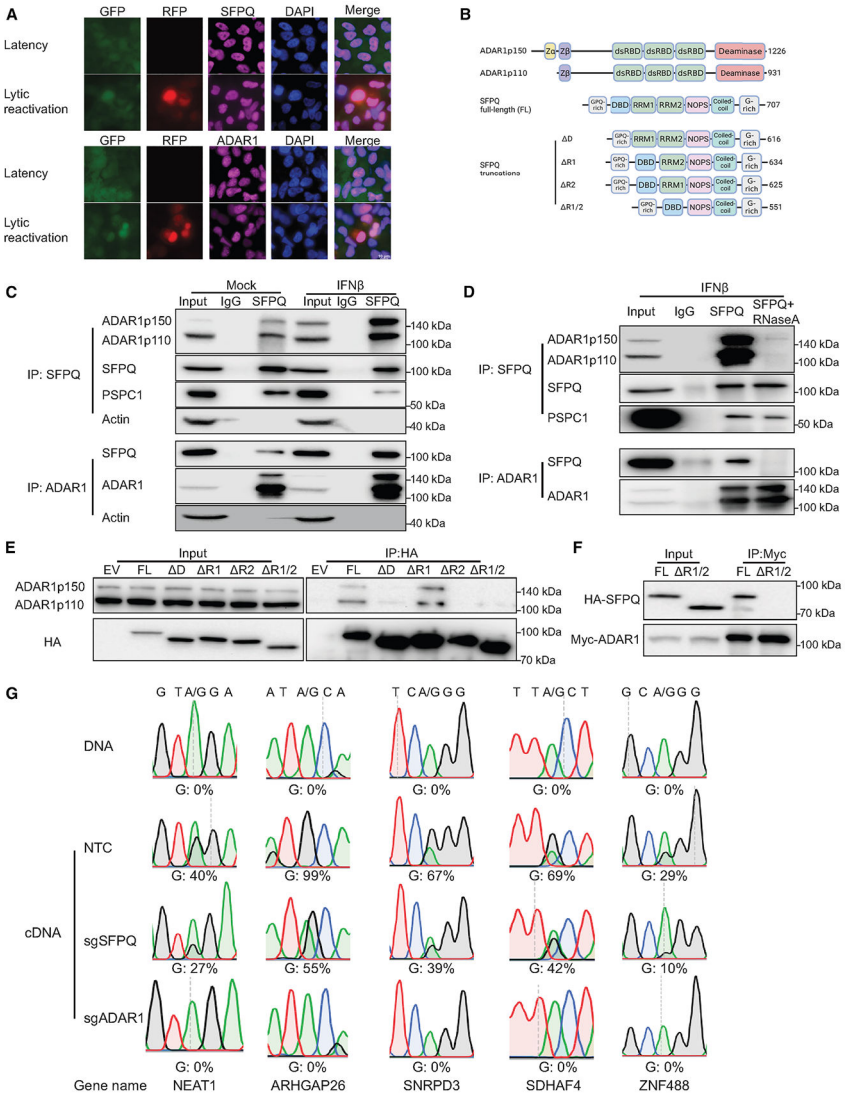

Figure 3. SFPQ interacts with ADAR1 isoforms and affects A-to-I RNA editing

(A and B) Cellular localization of SFPQ and ADAR1 in iSLK.219 cells. iSLK.219 cells were treated with DMSO and 0.2 μg/mL Dox for 48 h and then processed for immunofluorescence. Scale bars, 10 μm. (B) Schematic structure of ADAR1 p110 and P150 isoforms, SFPQ full-length (FL) and truncated mutants.

(C) HEK293T cells were treated with or without IFNβ for 24 h. The cell lysates were immunoprecipitated with SFPQ (top) or ADAR1 (bottom) antibodies and then immunoblotted with the indicated antibodies.

(D) HEK293 cells were treated with IFNβ for 24 h. The cell lysates were incubated with and without RNase A and then immunoprecipitated with SFPQ (top) and ADAR1 (bottom). The immunoprecipitates were immunoblotted with the indicated antibodies.

(E) HA-tagged FL SFPQ and truncated mutants were transfected individually into HEK293T cells. Cell lysates were immunoprecipitated with anti-HA beads and then immunoblotted with the indicated antibodies.

(F) HEK293T cells were transfected with Myc-tagged ADAR1 together with either FL SFPQ or an SFPQ mutant lacking both RRM1 and RRM2 domains. Cell lysates were immunoprecipitated with anti-Myc beads and subsequently immunoblotted with the indicated antibodies.

(G) HUVEC cells constitutively expressing Cas9 were transfected with NTC and SFPQ sgRNA. RNA was extracted from the cells and then amplified to cDNA. Genomic DNA was extracted from wild-type HUVEC cells. Sanger sequencing chromatograms illustrate different editing sites in the genomic DNA and cDNA as described earlier. The frequency of A-to-G editing was estimated based on Sanger sequencing with EditR. The data are representative of three independent experiments.

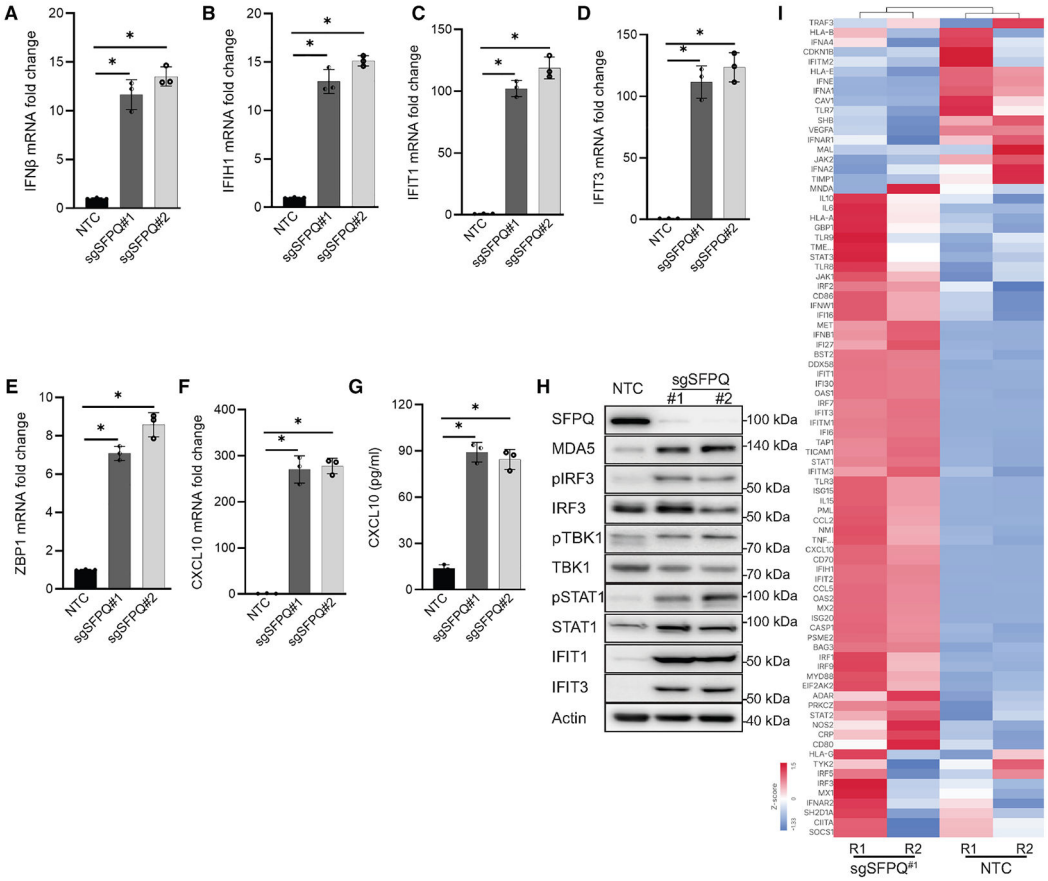

Figure 4. SFPQ deficiency induces the type I IFN response

(A–F) The mRNA expression levels of IFNβ (A), IFIH1(B), IFIT1(C), IFIT3(D), ZBP1(E), and CXCL10 (F) were measured by real-time PCR.

(G) CXCL10 protein levels in the supernatants were determined by ELISA.

(H) Cell lysates were collected, and western blots were performed with the indicated antibodies. For total IRF3, TBK1, and STAT1 levels, the western blot for phospho-IRF3, phospho-TBK1, and phospho-STAT1 was stripped and reprobed with antibodies against total IRF3, TBK1, and STAT1.

(I) Heatmap of human type I IFN transcripts. RNA was extracted from NTC- and sgSFPQ#1-treated HUVEC cells, and the mRNA level of the indicated genes were analyzed using the human type I IFN response RT2 Profiler PCR Array. R1 and R2 indicate data from duplicate samples. Red indicates high gene expression level, and blue indicates low or no gene expression level.

HUVEC cells constitutively expressing Cas9 were transfected with non-targeting control (NTC) or with two different sgRNAs targeting SFPQ for 4 days. The data in (A)–(H) are representative of three independent experiments. The data in (I) are representative of two independent experiments. The bar charts are presented as mean ± SD. *$p < 0.05$ by Student's *t* test.

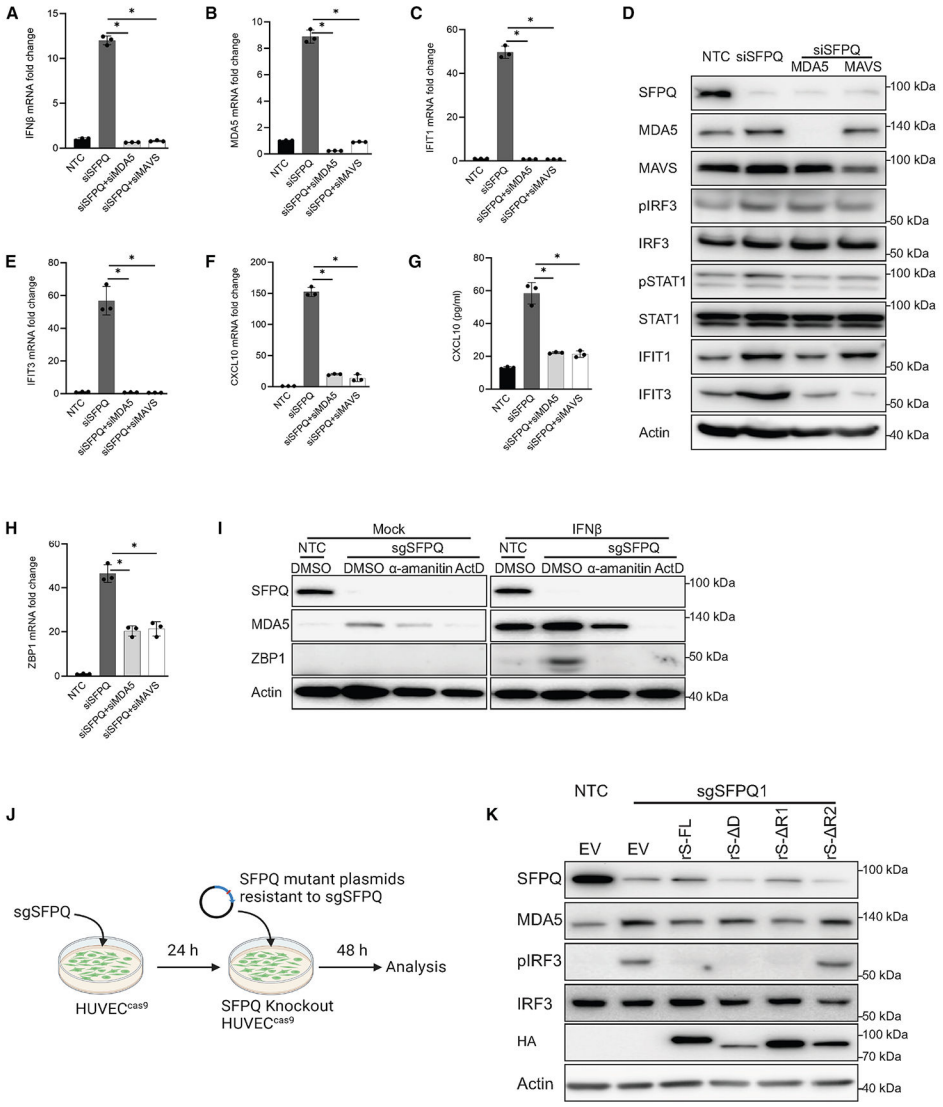

Figure 5. MDA5 contributes to SFPQ deficiency-induced lethal type I interferon response

(A–I) HUVEC cells were transfected with the indicated siRNA for 4 days. The fold induction of mRNA expression levels was measured by real-time PCR (A–C and E–H). The protein expression level was detected by western blot and ELISA (D and G). For total IRF3 and STAT1 levels, the western blots for phospho-IRF3 and phospho-STAT1 were stripped and reprobed with antibodies against total IRF3 and STAT1 in (D). HUVEC-Cas9 cells were transfected with NTC and SFPQ sgRNA for 48 h (I). The cells were then treated with IFNβ for a total of 24 h. After the initial 12 h of IFNβ treatment, the cells were co-incubated with actinomycin D or α-amanitin for the remaining 12 h. Cell pellets were harvested for western blot analysis.

(J and K) HUVEC-Cas9 cells were transfected with NTC and SFPQ sgRNA for 24 h and then the cells were transfected with empty plasmid (EV), as well as full-length and truncated mutant SFPQ plasmids for 48 h to reconstitute SFPQ and its mutants. Schematic depicting the process is shown in (J). Cell lysates were collected, and western blots were performed with the indicated antibodies. For total IRF3 levels, the western blot for phospho-IRF3 was

stripped and reprobed with an antibody against total IRF3 (K). The data are representative of three independent experiments. The bar charts are presented as mean ± SD. *$p < 0.05$ by Student's *t* test.

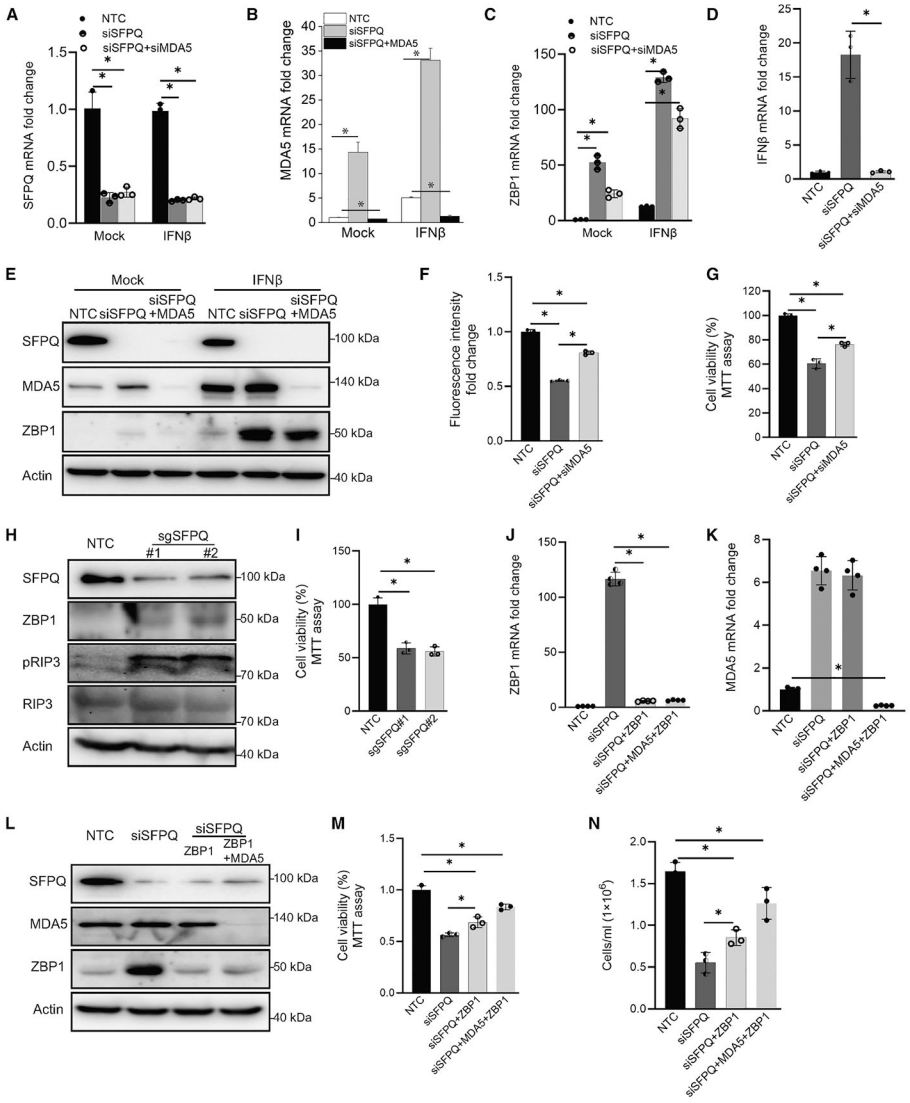

Figure 6. Depletion of SFPQ causes cell growth inhibition

(A–D) HUVEC cells were transfected with the indicated siRNA, and the fold induction of mRNA expression levels was measured by real-time PCR.

(E) Protein expression levels were detected by western blot with the indicated antibodies.

(F) Live cells were stained with calcein green dye, and the fluorescent signals were measured with a plate reader. Fluorescent intensity serves as a marker for live cells.

(G) Cell proliferation/viability was also determined at 5 days post-transfection by MTT assay.

(H and I) EA.hy926-Cas9 cells were transfected with NTC or two different sgRNA targeting SFPQ for 6 days, cell lysates were collected, and western blots were performed with the indicated antibodies. For total RIP3 levels, the western blot for phospho-RIP3 was stripped and reprobed with an antibody against total RIP3 (H). Cell proliferation was also determined by MTT assay (I).

(J–N) EA.hy926 cells were transfected with NTC and SFPQ alone or together with ZBP1 or ZBP1 plus MDA5 siRNA for 6 days. The mRNA expression levels of ZBP1 (J) and

MDA5 (K) were measured by real-time PCR. Protein expression levels were detected by western blot with the indicated antibodies (L). Cell proliferation/viability was determined by MTT assay (M). Cells were counted following Trypan Blue staining (N). The data are representative of three independent experiments. The bar charts are presented as mean ± SD. *$p < 0.05$ by Student's t test.

KEY RESOURCES TABLE

REAGENT or RESOURCE	SOURCE	IDENTIFIER
Antibodies		
SFPQ	Bethyl Laboratories	A301-320A; RRID: AB_937991
ORF45	Thermo Fisher	Cat# MA5-14769; RRID: AB_10999794
K8α	Santa Cruz	Cat# sc-57889; RRID: AB_783765
vIL6	This laboratory	N/A
pIRF3	Abcam	Ab76493; RRID: AB_1523836
IRF3	Cell signaling	4302; RRID: AB_1904036
pTBK1	Cell signaling	5483; RRID: AB_10693472
TBK1	Cell signaling	3504; RRID: AB_2255663
MDA5	Cell signaling	5321; RRID: AB_10694490
MAVS	Cell signaling	3993; RRID: AB_823565
ZBP1	Cell signaling	60968; RRID: AB_7299599
ADAR1	Cell signaling	81284; RRID: AB_3068597
pSTAT1	Cell signaling	9167; RRID: AB_561284
STAT1	Cell signaling	14994; RRID: AB_2737027
IFIT1	Cell signaling	14769; RRID: AB_2783869
IFIT3	Cell signaling	87781; RRID: AB_3717248
PSPC1	Santa Cruz	sc-374181; RRID; AB_1098076
NONO	Cell signaling	10162; RRID: AB_3714908
B-Actin	Santa Cruz	Cat# sc-47778; RRID: AB_626632
Anti-rabbit IgG HRP	Cell signaling	Cat# 7074S; RRID: AB_2099233
Anti-mouse IgG, HRP	Cell signaling	Cat# 7076S; RRID: AB_330924
Chemicals, Peptides, and Recombinant Proteins		
Lipofectamine RNAiMAX	Invitrogen	Cat# 13778150
Lipofectamine 2000	Invitrogen	Cat# 11668019
Doxycycline Hydrochloride	Fisher Scientific	Cat# BP26535
Opti-MEM	Gibco	REF# 31985-070
2-Mercaptoethanol	Gibco	REF# 21985-023
Tetracycline-free FBS	Clontech	Cat# 631106
Puromycin	Corning	REF# 61-385-PA
Hygromycin B	Corning	REF# 30-240-CR
Blasticidin	Invivogen	REF# ant-bl-1
Geneticin	Gibco	REF# 10131-035
5X siRNA buffer	Fisher Fisher	REF# B-002000-UB-100
DMEM	Corning	REF# 17-205-CV
RPMI 1640	Corning	REF# 10-040-CV
Pierce™ IP Lysis Buffer	Thermo Fisher	Cat# 87787
Protease inhibitor cocktail	Sigma-Aldrich	Cat# 11697498001
Pierce™ Anti-HA Magnetic Beads	Thermo Fisher	Cat# 388836
Dynabeads™ Protein G	Thermo Fisher	Cat# 10004D

REAGENT or RESOURCE	SOURCE	IDENTIFIER
ViraPower Lentiviral Packaging Mix	Invitrogen	Cat# K497500
Q5 High-Fidelity DNA Polymerase	NEB	Cat# M0491S
Trypan Blue solution	Thermo Fisher	Cat# 15250061
Calcein AM	Thermo Fisher	Cat# C1430
Critical Commercial Assays		
RNeasy Plus Mini Kit	Qiagen	Cat# 74136
DNeasy Mini Kit	Qiagen	Cat# 69506
Oligotex mRNA Mini Kit	Qiagen	Cat# 70022
Plasmid Plus Midi Kit	Qiagen	Cat# 12943
MTT assay	Abcam	Cat3 ab211091
SensiFAST cDNA Synthesis Kit	Bioline	Cat# BIO-65054
SensiFAST SYBR Lo-ROX Kit	Bioline	Cat# BIO-94050
IFN-beta DuoSet ELISA kit	R&D Systems	Cat# DY8234-05
CXCL10/IP-10 ELISA kit	Abcam	Cat# ab173194
Q5 Site-Directed Mutagenesis Kit	NEB	Cat# E0554S
Cell Line Nucleofector Kit V	Lonza	Cat# VCA-1003
NEBbuilder HiFi DNA Assembly Cloning Kit	NEB	Cat# E5520S
Human Interferons and Receptors RT2 Profiler PCR Array	Qiagen	Cat# PAHS-064Z
Deposited Data		
RNA and WGS sequencing data	NCBI BioProject database: https://www.ncbi.nlm.nih.gov/bioproject	Accession # is PRJNA1433810
Experimental Models: Cell Lines		
Human: iSLK.219	Don Ganem laboratory	Myoung and Ganem[22]
Human: iSLK.219-cas9	This paper	N/A
Human: Trex-BCBL-1	Jae Jung laboratory	N/A
Human: HUVEC-cas9	This paper	N/A
Human: 293FT	Thermo Fisher	Cat# R70007
Oligonucleotides		
See Tables S2 and S3 for oligonucleotide information	N/A	N/A
siRNA, shRNA, and sgRNA sequences (list in Table S2)	N/A	N/A
Primers sequences (list Table S3)	N/A	N/A
Recombinant DNA		
HA-SFPQ	Addgene	166959
HA- SFPQ-ΔDBD	This paper	N/A
HA- SFPQ-ΔRRM1	This paper	N/A
HA- SFPQ-ΔRRM2	This paper	N/A
HA- SFPQ-ΔRRM1/2	This paper	N/A
Edit-R Lentiviral Cas9 nuclease	Dharmacon	CAS11916
Software and Algorithms		
Partek Flow Genomic Analysis	Partek	https://ftp.partek.com/flow/login.xhtml

REAGENT or RESOURCE	SOURCE	IDENTIFIER
CLC Genomics Workbench 23	QIAGEN	N/A
LAS X	Leica	N/A
Origin 9	Origin Lab	N/A
Illustrator 2000	Adobe	N/A